Classification and Prediction of Human Blood Cells Using Artificial Intelligence and Advanced Image Processing Techniques

Ahmad S. Lateef (1), Ahmed J. M. Al-Zuhairi (1), Mohammed Y. Kamil (1)

- ¹ Mustansiriyah University, College of Science, Baghdad, Iraq.
- ² Department of Physiology and Medical Physics, College of Medicine, University of Diyala, Diyala, Iraq.

Abstract

Background: Accurate blood cell classification is essential for diagnosing and monitoring blood disorders. Manual blood evaluation is cumbersome and subject to disagreement among specialists, which can negatively impact diagnostic reliability.

Objectives: This study aims to develop an automated deep learning framework for accurate classification of major blood cell types, especially basophils, red blood cells, and bone marrow cells, to enhance the accuracy and efficiency of clinical diagnosis.

Patients and Methods: A set of publicly available, high-resolution blood smear images obtained from a specific patient cohort with distinct genetic properties was analyzed, with standardized preprocessing applied to address variance. Multiple AI-based classification strategies were developed, and all models were evaluated on an independent test set using overall accuracy, precision, recall, and F1 score.

Results: Wavelet scattering combined with an SVM delivered the strongest overall performance, surpassing both the custom CNN and ResNet variants. It achieved a near-perfect separation of basophils and erythroblasts and only occasional confusion with myeloblasts. These results highlight the sensitivity of the wavelet scattering method to subtle morphological differences in blood cells.

Conclusion: This study highlights how machine learning-based image analysis techniques can reliably and accurately classify blood cells, reducing the need for the subjective manual interpretation that characterizes traditional microscopy. There is potential for increasing the accuracy of early diagnosis and simplifying patient treatment plans for hematological disorders by integrating these automated systems into standard clinical practice.

Keywords: Hematological Diagnostics, Blood Cell Classification, Wavelet Scattering Transform, Transfer Learning.

OPEN ACCESS

Correspondence: Ahmad S. Lateef Email: a97s21@uomustansiriyah.edu.iq Copyright: ©Authors, 2024, College of Medicine, University of Diyala. This is an open access article under the CC BY 4.0 license (http://creativecommons.org/licenses/by/4.0/) Website:

https://djm.uodiyala.edu.iq/index.php/djm

Received: 10 May 2025 Accepted: 16 September 2025 Published: 25 October 2025

Introduction

The diagnosis and treatment of blood disorders, such as leukemia and bone marrow dysplasia, rely on blood cell classification; however, traditional microscopic examination remains time-consuming and subject to interdisciplinary variation. Advanced artificial intelligence and image processing techniques can overcome these limitations by providing objective and reproducible analyses of cellular characteristics, enabling early detection of subtle morphological changes, and helping guide individual treatment decisions. To demonstrate better outcomes, accuracy and consistency than

traditional microscopy, we create and validate an AI-driven framework in this study for the automated classification of basophils, erythroblasts, and myeloblasts in high-resolution blood smear images (1-3).

Deep learning frameworks and sophisticated computational techniques have emerged as potent remedies for these problems in recent years (4). For various tasks in biomedical image analysis, CNNs, transfer learning frameworks, and autoencoder-based cascades have been widely utilized (5-8). These methodologies have achieved high precision in recognizing the populations of various leukocytes, providing more objective and reproducible alternatives to manual methods. Even with these advances, the classification of basophils, erythroblasts, and myeloblasts remains challenging because their histological features are very delicate, as there are no comprehensive, properly cataloged data sets (9-16). Consequently, a successful computerized classification scheme would significantly enhance diagnostic precision, ultimately leading to earlier diagnosis and more targeted therapies (17-20).

This work primarily aims to address this shortcoming by developing and validating a custom-designed deep learning algorithm for classifying basophils, erythroblasts, and myeloblasts from microscopic images. By embracing the latest image processing methodologies and advanced neural network designs, the strategy aims to minimize subjectivity in morphological evaluation and enhance consistency during cell classification. In the process, we confront the specific challenges related to these cells while building upon the promising results from the most recent studies. Following this introductory section, the paper proceeds as outlined below.

First, a comprehensive review of related work is provided, summarizing current methodologies and their inherent limitations. Next, the proposed methodology, including the network design and data augmentation strategies employed to address data scarcity and morphological overlap, is described in detail. Finally. we present results validate experimental that the effectiveness of our approach and discuss the potential implications for clinical hematological diagnostics and future research directions. Arabyarmohammadi et al. (2022) trained a deep model to segment myeloblast chromatin and extracted 214 texture/shape features. After LASSO and Cox regression refinement, their risk score correlated with relapse-free survival (AUC 0.71) in AML and MDS post-transplant patients, demonstrating a reproducible alternative to manual cytology (21). In addition, Guo et al. (2022) developed a deep classifier with a "rejected option" to flag ambiguous bone marrow images. By quantitatively measuring morphological features, the system abstains from uncertain cases, reducing misclassification and directing them to expert review (22). Jarjees et al. (2022) developed a VGG-19 transfer-learning pipeline using an augmented dataset comprising seven blood cell classes. Their CNN achieved 98 % overall accuracy, standardizing leukocyte classification and minimizing dependence on expert interpretation (23). Tarquino et al. (2023) introduced a cascade of one-class variational autoencoders to distinguish four pathological bone marrow subtypes. Trained on 26,000 openaccess images, the model achieved 93.8% accuracy, outperforming benchmarks ResNext, ResNet-50, Xception, and CoAtNet (24). Consensus criteria for acute and chronic basophilic leukemias were established, defining "hyperbasophilia" (≥1,000 basophils/µL) and standardizing diagnoses to enhance clinical reproducibility across hematologic malignancies (25). A CNN with specialized layers and data augmentation was designed to detect AML in high-resolution images. The system delivered high accuracy and reliability, demonstrating

versatility for other overlapping cell types and accelerating diagnostic workflows (26).

Patients and Methods

Dataset description: A portion of a publicly available Kaggle dataset was utilized in this study. The dataset comprises 5,000 high-resolution microscopic blood cell images evenly distributed across five classes (1,000 images per class) from different countries. Each image meets the following technical specifications:

minimum resolution of 1024×1024 pixels, Wright-Giemsa staining, acquisition at 100× oil immersion (equivalent to 1000× total magnification), 24-bit RGB color, and multiple focal planes per sample. Given the computational demands associated with training AI algorithms on such high-resolution data, only a subset of the dataset was employed for training, specifically, three classes with 100 images per class. A portion of the dataset is depicted in Figure 1.

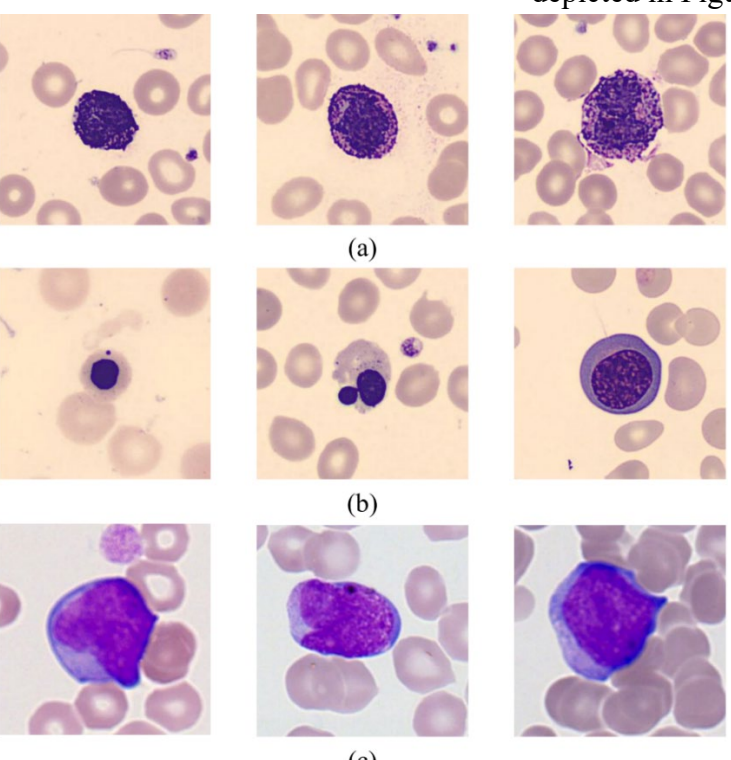


Figure 1. Samples of the dataset: (a) Basophil cells; (b) Erythroblast; and (c) Myeloblast.

Data preparation: The study employed a publicly available dataset of blood smear images. The original dataset was provided as a compressed archive (e.g., BloodSmearImages.zip) and was extracted to a designated working directory. The images are in RGB format with a common size of 1024×1024 pixels, which leads to resizing the images to 400×400 pixels. To facilitate data management and ensure proper labeling, an Image Datastore was created; labels were automatically assigned based on the folder

names. The dataset comprises 100 images uniformly distributed across three classes corresponding to specific parasitic infections (basophil, erythroblast, and myeloblast), with 100 images per class.

To ensure balanced class representation, the dataset was split into training and hold-out (test) sets using a 70:30 ratio. Randomization was controlled via a fixed random seed to guarantee reproducibility. The entire set of training and test images was loaded into memory, which permitted rapid access during feature extraction and classifier training.

Feature extraction using wavelet scattering technique: Accurate feature extraction is crucial due to the dataset's small size and diversity. To address this challenge, a twolayer wavelet dispersion transform was applied to extract low-contrast, translationinvariant feature descriptors from highresolution images. The network was designed to accommodate input images of 400 × 400 pixels, with a 40-pixel invariance scale selected to ensure robustness against subtle translational shifts and shape distortions. Two wavelets per octave were used in the first dispersion layer to capture fine details. In contrast, one wavelet per octave was employed in the second layer to downscale the resolution hierarchically. To enable the model to adapt to angular variations in cellular structures, two rotational transforms were incorporated into each dispersion layer to account for orientation diversity. The outcome of these stages is a robust set of dispersion parameters, including successive wavelet convolutions. nonlinear parameter transformations, and local averaging via lowpass filtering. These parameters serve as highlevel discriminative representations enhance the model's ability to distinguish between normal and pathological cell types, even in images exhibiting subtle variations that complicate discrimination.

Classification using support vector machine (SVM): Following feature extraction, the scattering coefficients were used as inputs to a Support Vector Machine (SVM) classifier. Recognized for their effectiveness in high-dimensional spaces and limited-sample scenarios, SVMs were chosen to robustly discriminate among the classes. In our implementation, a multiclass SVM was constructed using the one-vs-all strategy (or error-correcting output codes) to generalize the binary decision-making process inherent

in SVMs to a multiclass classification problem.

Hyperparameters for the SVM, including the choice of kernel (e.g., linear or radial basis function), regularization parameters, and other tuning parameters, were optimized using cross-validation on the training set. This approach ensured that the classifier maintained high generalizability and minimized the risk of overfitting. The classifier's performance was subsequently assessed on the reserved test set using standard metrics, including accuracy, precision, recall, and F1-score. Table 1 shows the hyperparameters of the SVM algorithm.

Table 1. Properties of the Wavelet feature extraction method.

Parameter	value	
KernelFunction	cubic polynomial kernel	
PolynomialOrder	3	
KernelScale	1	
BoxConstraint	314	
Standardize	True	
KFold	5	

Deep convolutional neural network: The results of the Water sorption of the zirconium mixed with PVA decreased in the study group compared to the control group, as shown in Table 2. It was demonstrated that water sorption results show

a significant difference in the study group at all curing times (1-2-5-10-15-20 sec), while showing a non-significant difference in the control group at all curing time intervals.

Deep convolutional neural network: The custom Convolutional Deep Network is engineered to learn discriminative features directly from input images by employing a structured architecture that begins with an input layer where images are resized to a fixed resolution (e.g., 300×300 pixels) and accepted in 24-bit RGB format. The network then utilizes a series of convolutional blocks for feature extraction; each block typically comprises a convolutional layer with small receptive fields (such as 3×3 filters) to scan the input feature maps, followed by batch normalization layers to stabilize and accelerate training, ReLU

activation functions to introduce non-linearity, and max pooling layers to down sample the feature maps- thereby reducing spatial dimensions and capturing translational invariance. After several such blocks, a global average pooling layer aggregates these high-level features, summarizing the learned spatial representations into a fixed-length feature vector. This vector is further processed

through one or two fully connected dense layers that incorporate dropout to prevent overfitting, given the high capacity of the network relative to the dataset size. Finally, the architecture culminates in a fully connected SoftMax output layer, which maps the refined features to class probabilities corresponding to the various blood cell categories.

Table 2. Architecture of the custom deep CNN.

Layer (type)	Output Shape	Number of parameters
conv2d_4 (Conv2D)	(None, 400, 400, 16)	2368
batch normalization 4	(None, 400, 400, 16)	64
re_lu_4 (ReLU)	(None, 400, 400, 16)	0
conv2d 5 (Conv2D)	(None, 400, 400, 20)	2900
batch normalization 5 (Batch)	(None, 400, 400, 20)	80
re_lu_5 (ReLU)	(None, 400, 400, 20)	0
max pooling2d 2 (MaxPooling2)	(None, 100, 100, 20)	0
flatten_2 (Flatten)	(None, 200000)	0
dense_2 (Dense)	(None, 3)	600003
softmax_2 (Softmax)	(None, 3)	0
Total params: 605415, Trainable params: 605343, Non-trainable params: 72		

The network was trained using stochastic gradient descent (or an alternative optimizer such as Adam) with appropriate learning rate scheduling and weight regularization (e.g., L2 weight decay). Hyperparameters, including mini-batch size, learning rate, dropout ratio, and number of epochs, were empirically set, followed by cross-validation to ensure robust performance and mitigate overfitting. Data augmentation techniques (e.g., rotation, scaling, or flipping) were applied during training to expand the effective dataset and further enhance the model's generalization.

ResNet network: ResNet, or Residual Network, is a highly effective deep learning model known for its ability to train very deep neural networks by addressing the vanishing gradient problem through skip connections. In our work, we used a pretrained version of ResNet, specifically ResNet-50, because of its strong performance in image classification

tasks. The core idea behind ResNet lies in its residual blocks, which include shortcut connections (also called identity mappings) that skip over one or more layers. These connections allow the network to learn residual functions relative to the input, making it easier to train deeper models by reducing the degradation problem.

Stacking multiple residual blocks can enable the network to obtain high-level representations from low-level textures progressively. This functionality is very effective for recognizing faint blood cell morphology cues. Transfer learning was used to allow the pretrained ResNet model to learn blood cell classification. It allowed us to leverage strong feature representations learned on the vast ImageNet dataset. Early layers of the network extract general visual features that are widely applicable, so we left most of them unchanged.

For a certain number of classes in the dataset, we replaced the classification layer with a different fully connected softmax layer, and we then adjusted the learning rate. By doing this, it was able to stay close

$$P = \frac{\text{TP}}{\text{TP} + \text{FP}}$$

- Recall (R) measures the ability of the model to capture all actual positive instances (27):

$$R = \frac{\text{TP}}{\text{TP} + \text{FN}}$$

- F1-Score is the harmonic mean of precision and recall, providing a balanced measure (27):

$$F1 = 2 \times \frac{P \times R}{P + R}$$

A confusion matrix was constructed during the qualitative analysis to assess the performance of the models in each category, which helps identify patterns of misclassification and highlights areas that require improvement in each model.

Results

Study design:

Both models were implemented in MATLAB. The custom network was constructed using the deep learning primitives available in the MATLAB Deep Learning Toolbox, while the pretrained ResNet model was adapted using MATLAB's transfer learning capabilities. The environment facilitated rapid prototyping, hyperparameter exploration, and performance evaluation using standard metrics such as accuracy, precision, recall, and F1-score.

Classification via wavelet scattering features using SVM: Figure 2 shows the confusion matrix obtained from the wavelet scattering feature extraction and SVM classification approach, which reveals an overall high performance discriminating blood cell types. For the three classes under investigation- basophils, erythroblasts, and myeloblasts- the classifier achieved near-perfect Specifically, both accuracy. basophils erythroblasts were classified with 100% accuracy, indicating that the scattering coefficients extracted from these cell images capture their distinctive morphological features very effectively. Myeloblasts, while also largely well-classified with

to the original and preserve only limited, yet significant, modifications introduced by the model's retraining for the particular domain. To enhance the model's resilience and generalization capabilities, we also employed regularization and data augmentation techniques. This led to the development of a functional and precise blood type classification system.

Evaluation: To conduct a comprehensive performance comparison of the methods adopted in this study, we ran each technique on a hold-out test dataset comprising 30% of the entire dataset. To evaluate the developed model, we used accuracy, precision, recall, and F1-score classification metrics. We computed each metric for each class and then averaged it with the macro average across all classes to obtain an overall assessment of the model's performance across all classes.

For reference:

- True Positives (TP): The number of samples correctly predicted as belonging to a given class.
- False Positives (FP): The number of samples incorrectly predicted to belong to the class.
- True Negatives (TN): The number of samples correctly identified as not belonging to the class.
- False Negatives (FN): The number of samples that were actually in the class but were misclassified as something else.

The evaluation metrics were computed using the following equations:

- Accuracy measures the proportion of all correct predictions (24):

$$Accuracy = \frac{TP + TN}{TP + TN + FP + FN}$$

- Precision (P) quantifies the correctness of positive predictions for a class (27):

29 out of 30 instances correctly identified, exhibited a single misclassification (incorrectly labeled as an erythroblast),

resulting in a slight reduction in metrics such as recall and F1-score for this class.

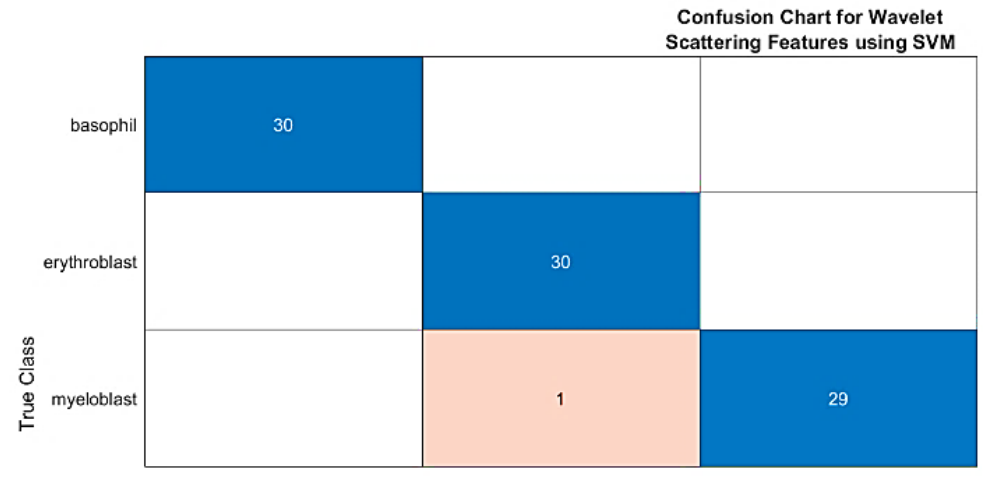


Figure 2. Confusion chart of Wavelet features using SVM.

The excellent performance for basophils and erythroblasts suggests that the wavelet scattering transform is successful in deriving translation-invariant and discriminative features that robustly represent morphological characteristics of these cells. The minor overlap observed between myeloblasts and erythroblasts, however, implies that in certain cases, the feature space representations of these two cell types may become similar. Such subtle overlaps are not entirely unexpected, given the inherent complexity in distinguishing cells that share comparable structural and textural attributes. The SVM classifier, when provided with these high-quality features, demonstrates effective discrimination across classes. Its decision boundaries appear to be well-calibrated, as evidenced by the high class-wise accuracies. the misclassification of one myeloblast highlights a potential area for

further refinement. Future work could explore more sophisticated feature fusion techniques that integrate additional descriptors (e.g., color histograms or morphological measurements) into the classification pipeline, or consider threshold adjustments and ensemble learning methods to more reliably resolve borderline cases.

Classification via deep CNN: The training of the deep CNN model was characterized by steady improvements in both accuracy and loss over successive epochs, as illustrated in Figure 3. Initially, the model achieved around 60% accuracy, and within several epochs, it rapidly improved, eventually stabilizing between 90% and 100%. Concurrently, the training loss started from a high value (approximately 9) and consistently decreased toward near-zero levels, reflecting effective optimization of network weights and a substantial reduction in the difference between predicted outputs and true labels.

Diyala Journal of Medicine

ORIGINAL RESEARCH Published: 25 October 2025 DOI: 10.26505/djm.v29i1.1463

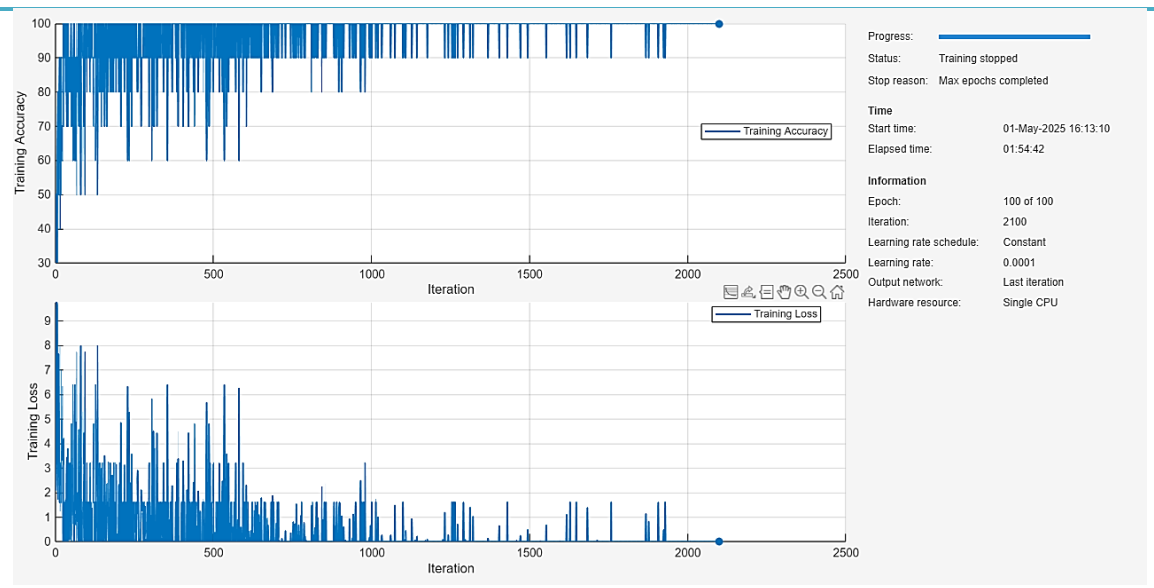


Figure 3. Training process of the deep CNN.

The network was trained for a total of 100 epochs, encompassing approximately 2100 iterations. A constant learning rate of 0.0001 was chosen, which contributed to the stable convergence observed, as it ensured gradual weight adjustments without causing erratic behavior in the loss or accuracy metrics. Notably, the training was executed on a single CPU, which may indicate either the modest scale of the dataset or a scenario where highend GPUs were not available. Despite these hardware constraints, the learning curves demonstrate that the model was able to effectively capture the morphological nuances in the blood cell images.

While minor fluctuations in training accuracy are common in mini-batch gradient descent due to inherent stochasticity, the overall upward trend in accuracy and corresponding decline in loss confirm the model's ability to learn relevant features. The training process was allowed to complete all 100 epochs, reaching a point of convergence where the loss stabilized and the accuracy plateaued, without the implementation of early stopping mechanisms.

The confusion matrix for the deep CNN model reveals near-perfect classification performance overall, with 100% accuracy for both basophils and myeloblasts. In comparison, erythroblasts show a slightly lower accuracy of 86.7% (26 out of 30 correctly classified, with 4 misclassified as basophils), as illustrated by Figure 4. When normalized by true class, basophils and myeloblasts maintain perfect recognition. In contrast, the rowwise accuracy for erythroblasts indicates that a small subset is misinterpreted, likely due to subtle morphological similarities to basophils, despite their distinctive features. Analysis of column-wise normalization shows that approximately 88.2% of samples predicted as basophils are indeed basophils, with the remainder being erythroblasts, underscoring a slight overlap in the feature space between these two classes. These observations suggest that while the deep CNN effectively distinguishes the majority of blood cell types, there remains an opportunity for further refinement, potentially through enhanced feature engineering, increased data augmentation, or additional model tuning to differentiate erythroblasts from basophils better and improve the overall robustness of the classifier in clinical diagnostics.

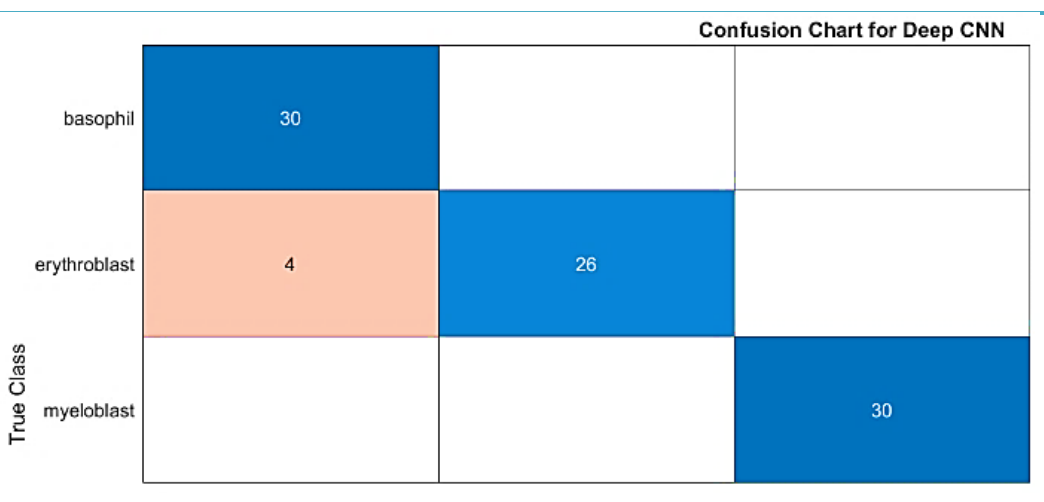


Figure 4. Confusion chart of the deep CNN.

Classification via transfer learning using **ResNet:** The training process of the ResNet model was both robust and efficient, as demonstrated by the steady evolution of key performance metrics over 2100 iterations and 100 epochs, as shown in Figure 5. Initially, the training accuracy rapidly increased from a moderate value, quickly approaching and then maintaining near 100% accuracy, indicating that the network's residual connections were highly effective in facilitating deep feature extraction and mitigating the vanishing gradient problem. Concurrently, the training loss decreased sharply from an initial high value and plateaued at very low levels, with only minor fluctuations that are typical in mini-batch optimization. This convergence was achieved using a constant learning rate of 0.0001, ensuring gradual yet consistent weight updates that contributed to the model's stable performance over time. Notably, the entire training process was executed on a single CPU, suggesting an efficient use of computational resources despite the complexity of the ResNet architecture. Overall, the training results indicate that the

The ResNet model successfully learned the underlying patterns in the data, as reflected in its high accuracy and low loss by the end of training, thereby affirming its potential for effective generalization to unseen samples.

Figure 6 displays the confusion matrix for the ResNet model, indicating a high level classification accuracy across the three blood cell categories. Specifically, basophils and myeloblasts classified with 100% are accuracy, while erythroblasts achieve a slightly lower accuracy of 90%, with 3 out of 30 instances misclassified as basophils. This pattern suggests that although the deep architecture of ResNet effectively captures the discriminative features necessary for accurate classification, there exists a subtle overlap between the feature representations of erythroblasts and basophils. Such overlaps may be due to inherent morphological similarities in the texture or structure of the cells. Overall, these results attest to the robustness of the transfer learning approach using ResNet while also highlighting an opportunity for further refinement in distinguishing closely related cell types.

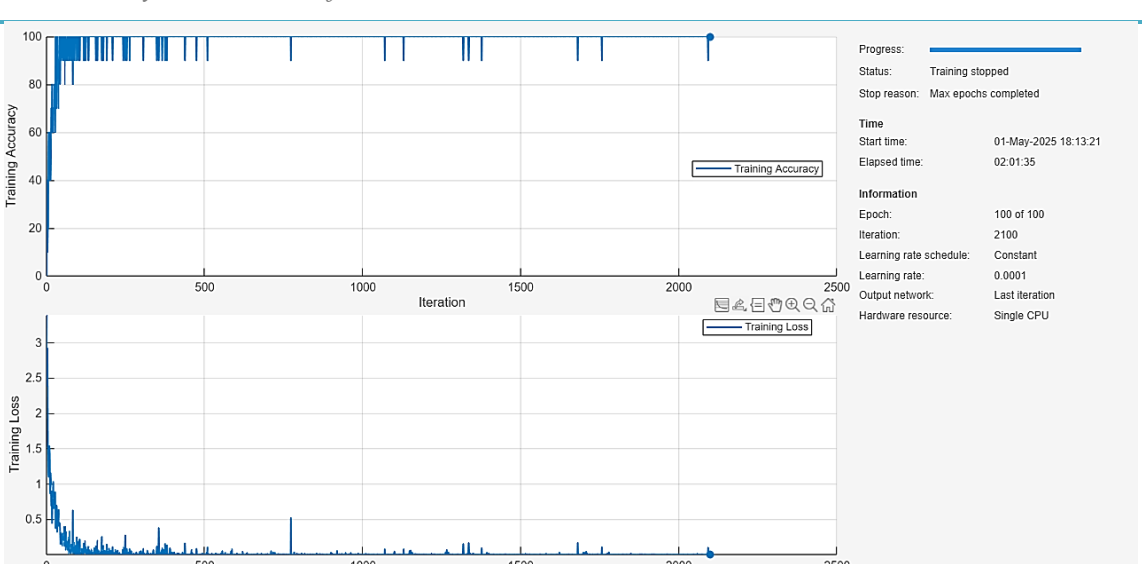


Figure 5. Training process of the ResNet method.

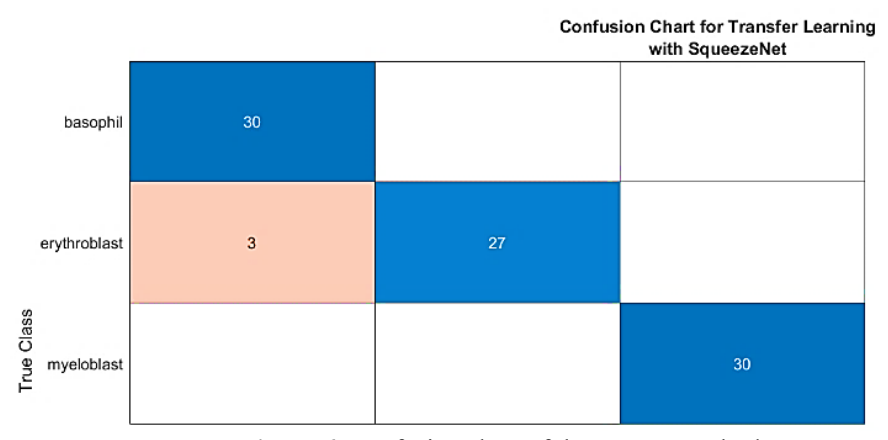


Figure 6. Confusion chart of the ResNet method.

Clinical integration and validation: To transition from a research prototype to a routine diagnostic tool, our AI framework must be embedded seamlessly within existing digital pathology infrastructures. In a typical laboratory workflow, blood smear slides scanned by high-throughput slide scanners will be automatically conveyed to the AI engine through the Laboratory Information System (LIS). The model's cell-type predictions-including confidence scores-will be overlaid on the digital-pathology viewer, pathologists visualize enabling to annotations alongside their manual assessments. This integration minimizes

additional workflow steps and ensures that AI outputs augment, rather than disrupt, established diagnostic practices.

Effective adoption also hinges on user training and feedback mechanisms. Laboratory staff will participate in structured workshops and e-learning modules to learn how to interpret AI annotations, manage low-confidence or "rejected" outputs, and reconcile discrepancies between model predictions and expert opinions. Regular feedback sessions will capture user experiences and inform iterative refinements of both the AI model and the user interface, ensuring that the system evolves in alignment with clinical needs.

Finally, safeguarding patient data and ensuring long-

term performance stability is paramount. All image transfers will adhere to HIPAA and GDPR standards, employing end-to-end encryption and de-identification protocols. Post-deployment, a continuous monitoring framework will track metrics such as false-positive and false-negative rates, model drift, and override frequencies. These indicators will trigger scheduled retraining with newly annotated cases, guaranteeing that the AI system maintains its accuracy and reliability over time.

Discussion

Our findings demonstrate that all three approaches-wavelet scattering with SVM, custom deep CNN, and ResNet transfer learning-achieved strong performance in distinguishing between basophils, erythroblasts, and myeloblasts. However, important performance differences emerged among the methods. The wavelet scattering with the SVM approach achieved the highest overall accuracy (~98.9%), with perfect classification of basophils and erythroblasts and only a single misclassification among myeloblasts. The deep CNN achieved 95.6% overall accuracy, with slightly reduced performance for erythroblasts (86.7%), while the ResNet model performed between the two methods, reaching 96.7% accuracy with 90% correct classification of erythroblasts. These differences highlight that while deep learning architectures are effective, handcrafted feature extraction using wavelet scattering remains highly competitive in scenarios with limited datasets.

Comparing these results with prior studies underscores their significance. Jarjees *et al.* (23) reported 98% accuracy using a VGG-19 transfer learning pipeline for leukocyte classification, which is comparable to our

ResNet model but slightly lower than the wavelet scattering + SVM approach. Similarly, Khanam et al. (26) demonstrated high performance of CNNs in acute myeloid leukemia detection, yet their work also noted challenges in separating morphologically similar cell types-a limitation mirrored in our between misclassifications erythroblasts and basophils. Tarquino et al. (24) achieved 93.8% accuracy with a variational autoencoder cascade for bone marrow cell classification, which is lower than all three methods in our study. This indicates that both conventional machine learning (wavelet scattering + SVM) and transfer learning approaches are advantageous for small, specialized datasets.

Other investigations have also confirmed the challenge of differentiating morphologically overlapping cells. Arabyarmohammadi *et al.* (21) utilized texture-based deep models to stratify myeloblasts in AML and MDS, reporting strong prognostic accuracy while also highlighting issues with feature overlap. Likewise, Guo *et al.* (22) proposed a rejection-based classifier for bone marrow cells to handle ambiguous cases, which aligns with our observation that a small subset of erythroblasts was misclassified as basophils.

Our results, therefore, support the notion that robust, handcrafted descriptors, such as wavelet scattering coefficients, outperform deep CNNs and even transfer learning models when dataset size is constrained, as they capture subtle morphological patterns without requiring massive annotated datasets (28). At the same time, the promising results of ResNet (96.7% accuracy) suggest that deep hierarchical feature extraction can achieve reliable performance and may surpass handcrafted features when larger datasets and additional augmentation strategies are available.

Taken together, this study contributes to the growing evidence that AI-driven image analysis can enhance hematological diagnostics by providing high accuracy and reducing inter-observer variability. While some misclassifications remain, particularly between erythroblasts and basophils, our

comparative analysis shows that integrating wavelet-based descriptors with traditional classifiers remains a viable and powerful approach. Future work should investigate hybrid feature fusion strategies, as well as enriched datasets, to further improve erythroblast recognition and achieve robust, clinically deployable diagnostic support systems.

Conclusion

Our findings demonstrate that AI can effectively automate blood cell classification, reducing the subjectivity of manual microscopy. All three models-wavelet scattering with SVM, a custom CNN, and ResNet-achieved high accuracy (>95%), with the wavelet-SVM combination performing best (~98.9%). However, a limitation of this study is the genetic properties of our dataset, which differs from others and may impact model generalizability. Future research should expand datasets and incorporate genetic variability to strengthen clinical applicability. Despite this, our work confirms that AI-driven frameworks are promising tools for enhancing hematological diagnostics

Source of funding: This research did not receive any specific grant from funding agencies in the public, commercial, or not-forprofit sectors.

Ethical clearance: Ethical approval for this study was obtained from the Ethics Committee of the College of Science, Mustansiriyah University.

Conflict of interest: The authors declare that they have no known competing financial interests or personal relationships that could have appeared to influence the work reported in this paper.

Use of Generative Artificial Intelligence (AI): The authors state that they did not utilize any generative AI tools for creating or editing the language of the manuscript.

Acknowledgments: The authors would like to thank Mustansiriyah University, Baghdad, Iraq, for supporting the presented work.

References

- 1. Aby AE, Salaji S, Anilkumar KK, Rajan T. Classification of acute myeloid leukemia by pretrained deep neural networks: A comparison with different activation functions. Medical Engineering & Physics. 2025;135:104277. doi: https://doi.org/10.1016/j.medengphy.2024.104277.
- 2. He J, Xu X, Zhang Y, Jiang S, Lin Q, Zhang H, et al. Photoelectrochemical aptasensing and fluorescence imaging co-joint detecting MCF-7 cells in whole blood via an inertial separation microfluidic chip. Talanta. 2025;286:127488. doi: https://doi.org/10.1016/j.talanta.2024.127488.
- 3. Zhang X, Zhao Q, Zhu W, Liu T, Xie SH, Zhong LX, et al. The Association of Telomere Length in Peripheral Blood Cells with Cancer Risk: A Systematic Review and Meta-analysis of Prospective Studies. Cancer Epidemiology,

Biomarkers & Prevention. 2017;26(9):1381–90. doi: https://doi.org/10.1158/1055-9965.EPI-16-0968.

4. Li Y, Cai L, Lu Y, Lin C, Zhang Y, Jiang J, et al. Domain-invariant representation learning via SAM for blood cell classification. Pattern Recognition. 2026;170:112000.

 $\underline{https://doi.org/10.1016/j.patcog.2025.112000}.$

- 5. AlKindy B, Jamil OB, Al-Nayyef H, Alkendi W. A Machine Learning Approach for Identifying Five Types of Horizontal Ocular Disorders Using Haar Features. Al-Mustansiriyah Journal of Science. 2025;36(1):69–83. doi: https://doi.org/10.23851/mjs.v36j1.1597.
- 6. Lakshmi Narayanan K, Santhana Krishnan R, Harold Robinson Y, Vimal S, Rashid TA, Kaushal C, et al. Enhancing acute leukemia classification through hybrid fuzzy C means and random forest methods. Measurement: Sensors. 2025;39. doi: https://doi.org/10.1016/j.measen.2025.101876.
- 7. Radhi E, Kamil M. An Automatic Segmentation of Breast Ultrasound Images Using U-Net Model. Serbian Journal of Electrical Engineering. 2023;20(2):191–203. doi:

https://doi.org/10.2298/SJEE2302191R.

8. Radhi EA, Kamil MY. Breast tumor segmentation in mammography image via Chan-Vese technique. Indonesian Journal of Electrical Engineering and Computer Science. 2021;22(2):809–17. doi:

http://doi.org/10.11591/ijeecs.v22.i2.pp809-817.

- 9. Das S, Padmanaban K. Incremental learning for acute lymphoblastic leukemia classification based on
- hybrid deep learning using blood smear image. Computational Biology and Chemistry. 2025;118. doi: https://doi.org/10.1016/j.compbiolchem.2025. 108456.
- 10. Fukuyama S, Kumamoto S, Nagano S, Hitotsuya S, Yasuda K, Kitamura Y, et al. Detection of cancer cells in whole blood using a dynamic deformable microfilter and a nucleic acid aptamer. Talanta. 2021;228:122239. doi: https://doi.org/10.1016/j.talanta.2021.122239. 11. Igbal A, Ahmed MF, Suvon MNI, Shuvho SD. Fahmin A. Towards Efficient Segmentation and Classification of White Blood Cell Cancer Using Deep Learning. 2021 Emerging Technology in Computing, Communication and Electronics (ETCCE)2021. p. 1-6.
- 12. Kamil M, Hashem S. Segmentation of Chest X-Ray Images Using U-Net Model. Mendel. 2022;28(2):49-3.. doi: https://doi.org/10.13164/mendel.2022.2.049.
- 13. Keller A, Leidinger P, Borries A, Wendschlag A, Wucherpfennig F, Scheffler M, et al. miRNAs in lung cancer studying complex fingerprints in patient's blood cells by microarray experiments. BMC Cancer. 2009;9:353. doi: https://doi.org/10.1186/1471-2407-9-353.
- 14. Muduli D, Parija S, Kumari S, Hassan A, Jangwan HS, Zamani AT, et al. Deep learning-based detection and classification of acute lymphoblastic leukemia with explainable AI techniques. Array. 2025;26. doi: https://doi.org/10.1016/j.array.2025.100397.
- 15. Rahman SIU, Abbas N, Salman M, Ali S, Alkhayat A, Khan J, et al. Deep Learning and Artificial Intelligence-Driven Advanced Methods for Acute Identification Leukemia Lymphoblastic and Classification: **Systematic** Review. Computer Modeling Engineering Sciences. 2025;142(2):1199–231. doi:

http://dx.doi.org/10.32604/cmes.2025.057462.

- 16. Yasui K, Saito T, Ueda S, Shinohara K, Fukami Y, Sano T, et al. Sequential Changes in Circulating Tumor Cells in the Peripheral
- Blood of Pancreatic Cancer Patients with Preoperative Chemotherapy Using a New Immunocytology-Based, Light Microscopic CTC Detection Platform. Diagnostics (Basel). 2025;15(6). doi: https://doi.org/10.3390/diagnostics15060752.
- 17. Alsamri J, Alqahtani H, Al-Sharafi AM, Darem AA, Nazim K, Sattar A, et al. Computer-aided diagnosis of Haematologic disorders detection based on spatial feature learning networks using blood cell images. Scientific Reports. 2025;15(1):12548. doi: https://doi.org/10.1038/s41598-025-85815-4.
- 18. Chola C, Muaad AY, Bin Heyat MB, Benifa JVB, Naji WR, Hemachandran K, et al. BCNet: A Deep Learning Computer-Aided Diagnosis Framework for Human Peripheral Blood Cell Identification. Diagnostics. 2022;12(11):2815. doi: https://doi.org/10.3390/diagnostics12112815.
- 19. Mohamed H, Omar R, Saeed N, Essam A, Ayman N, Mohiy T, et al. Automated detection of white blood cells cancer diseases. 2018 First International Workshop on Deep and Representation Learning (IWDRL)2018. p. 48–54.
- 20. Radhi EA, Kamil MY. Anisotropic Diffusion Method for Speckle Noise Reduction in Breast Ultrasound Images. International Journal of Intelligent Engineering and Systems. 2024;17(2):621–31. doi: https://doi.org/10.22266/ijies2024.0430.50.
- 21. Arabyarmohammadi S, Leo P, Viswanathan VS, Janowczyk A, Corredor G, Fu P, et al. Machine Learning to Predict Risk of Relapse Using Cytologic Image Markers in Patients With Acute Myeloid Leukemia Posthematopoietic Cell Transplantation. JCO Clinical Cancer Informatics. 2022(6):e2100156. doi: https://doi.org/10.1200/cci.21.00156.
- 22. Guo L, Huang P, He H, Lu Q, Su Z, Zhang Q, et al. A method to classify bone marrow cells with rejected option. Biomedical Engineering / Biomedizinische Technik. 2022;67(3):227–36. doi: https://doi.org/10.1515/bmt-2021-0253.
- 23. Jarjees MS, Sheet SSM, Ahmed BT. Leukocytes identification using augmentation and transfer learning based convolution neural network. Telkomnika (Telecommunication Computing Electronics and Control).

2022;20(2):314–20. doi:http://doi.org/10.12928/telkomnika.v 20i2.23163.

24. Tarquino J, Rodriguez J, Alvarez-Jimenez C, Romero E. A One-Class Variational Autoencoder (OCVAE) Cascade for Classifying Atypical Bone Marrow Cell Sub-types. Cham: Springer Nature Switzerland; 2023. p. 725–34.

25. Valent P, Sotlar K, Blatt K, Hartmann K, Reiter A, Sadovnik I, et al. Proposed diagnostic criteria and classification of basophilic leukemias and related disorders. Leukemia. 2017;31(4):788–97. doi: https://doi.org/10.1038/leu.2017.15.

26. Khanam AS, Khan MH, Tabassum F, Ripa TA, Jabid T, Ali MS, et al. Classification of acute myeloid leukemia using convolutional neural network. International Conference on Green Energy, Computing and Intelligent Technology (GEn-CITy 2023)2023. p. 253–8.

27. Al-Obaidi FEM, Al-Saeed AJMA, Al-Zuhairi AJM. Self-Automatic Threshold Technique For Eye Pupil Detection. Journal of Optics (India). 2025. doi: https://doi.org/10.1007/s12596-025-02529-6.

28. Hindi RJ. Ensemble Machine Learning Approach for Anemia Classification Using Complete Blood Count Data. Al-Mustansiriyah Journal of Science. 2025;36(3):51–70. doi: https://doi.org/10.23851/mjs.v36i3.1709.

تصنيف وتنبؤ خلايا الدم البشرية باستخدام الذكاء الاصطناعي وتقنيات معالجة الصور المتقدمة

الحمد سعيد لطيف، ٢ احمد جبار محمد، المحمد يوسف كامل

الملخص

الخلفية: يعد التصنيف الدقيق لخلايا الدم أمرًا بالغ الأهمية لتشخيص وإدارة اضطرابات الدم. حيث أن التقييمات اليدوية التقليدية لمسحات الدم تتطلب جهدًا كبيرًا وتخضع للتباين بين المختصين، مما قد يهدد موثوقية التشخيص.

ا**لأهداف:** تهدف هذه الدراسة إلى تطوير والتحقق من إطار عمل آلي يعتمد على التعلم العميق لتصنيف أنواع خلايا الدم الرئيسية بدقة، وتحديدًا الخلايا القاعدية، والخلايا الأرومية الحمراء، والخلايا الأرومية النقوية، لتعزيز دقة وكفاءة التشخيص في الإعدادات السريرية.

المرضى والطرق: قمنا بتحليل مجموعة فرعية مختارة من صور مسحات الدم عالية الدقة المتاحة publicly ، مع تطبيق معالجة مسبقة موحدة لمعالجة مشكلة التباين. تم تطوير واستعراض استراتيجيات تصنيف متعددة مدعومة بالذكاء الاصطناعي، حيث تم تقييم جميع النماذج على مجموعة اختبار مستقلة باستخدام مقاييس الدقة الشاملة، والدقة، والاستدعاء، ودرجة F1.

النتائج: أظهرت تقنية "تبعثر الموجهات (Wavelet Scattering) "المقرونة بآلة المتجهات الداعمة (SVM) أقوى أداءً إجمالي، متجاوزة أداء كل من شبكة CNN المخصصة والنماذج المشتقة من .ResNet حيث حققت هذه الطريقة فصلًا شبه كامل للخلايا القاعدية والخلايا الأرومية المحراء، واقتصر ارتباكها النادر على الخلايا الأرومية النقوية. تؤكد هذه النتائج على حساسية طريقة تبعثر الموجهات للفروق الشكلية الدقيقة في خلايا الدم.

الاستنتاج: تسلط هذه الدراسة الضوء على كيفية قدرة تقنيات تحليل الصور القائمة على التعلم الآلي على تصنيف خلايا الدم بشكل موثوق ودقيق، مما يقلل من الاعتماد على التفسير اليدوي الذاتي الذي يميز الفحص المجهري التقليدي. يوجد إمكانية لزيادة دقة التشخيص المبكر وتبسيط خطط علاج المرضى الذين يعانون من اضطرابات دموية من خلال دمج هذه الأنظمة الآلية في الممارسة السريرية القياسية.

الكلمات المفتاحية: التشخيص الدموي، تصنيف خلايا الدم، تحويل تبعثر الموجهات، التعلم بالانتقال.

المؤلف المراسل: احمد سعيد لطيف

a97s21@uomustansiriyah.edu.iq الايميل:

تاريخ الاستلام: ١٠ أيار ٢٠٢٥

تاريخ القبول: ١٦ ايلول ٢٠٢٥

تاريخ النشر: ٢٠ تشرين الاول ٢٠٢٥

العلوم، الجامعة المستنصرية، بغداد، العراق. 2 قسم الفسلجة والفيزياء الطبية، كلية الطب، جامعة ديالي، ديالي، العراق.